Theoretical Studies of the Transition-State Structures and Free Energy Barriers for Base-Catalyzed Hydrolysis of Amides

Ying Xiong and Chang-Guo Zhan*

Department of Pharmaceutical Sciences, College of Pharmacy, University of Kentucky, 725 Rose Street, Lexington, Kentucky 40536

Received: May 22, 2006; In Final Form: September 26, 2006

The transition-state structures and free energy barriers for the rate-determining step (i.e. the formation of a tetrahedral intermediate) of base-catalyzed hydrolysis of a series of amides in aqueous solution have been studied by performing first-principle electronic structure calculations using a hybrid supermolecule-polarizable continuum approach. The calculated results and a revisit of recently reported experimental proton inventory data reveal that the favorable transition-state structure optimized for the tetrahedral intermediate formation of hydroxide ion-catalyzed hydrolysis of formamide may have three solvating water molecules remaining on the attacking hydroxide oxygen and two additional water molecules attached to the carbonyl oxygen of formamide. The calculated results have also demonstrated interesting substituent effects on the optimized transition-state geometries, on the transition-state stabilization, and on the calculated free energy barriers for the base-catalyzed hydrolysis of amides. When some or all of the hydrogen atoms of formamide are replaced by methyl groups, the total number of water molecules hydrogen-bonding with the attacking hydroxide in the transition state decreases from three for formamide to two for *N*-methylacetamide, *N,N*-dimethylformamide (DMF), and *N,N*-dimethylacetamide (DMA). The larger substituents of the amide hinder the solvent water molecules approaching the attacking hydroxide oxygen in the transition state and, therefore, destabilize the transition-state structure and increase the free energy barrier. By using the optimized most favorable transition-state structures, the calculated free energy barriers, i.e., 21.6 (or 21.7), 22.7, 23.1, and 26.0 kcal/mol for formamide, *N*-methylacetamide, DMF, and DMA, respectively, are in good agreement with the available experimental free energy barriers, i.e., 21.2, 21.5, 22.6, and 24.1 kcal/mol for formamide, *N*-methylacetamide, DMF, and DMA, respectively.

Introduction

The hydrolysis of an amide or a peptide bond is one of the most important types of reactions in chemistry and biochemistry and, therefore, has been intensively studied both by experiment[1−7] and in theory.[8−17] The dominant reaction pathway for amide hydrolysis in aqueous solution is dependent on the pH of the reaction solution. In acidic solution, the carbonyl oxygen may be protonated and the protonation is followed by nucleophilic attack of a water molecule, which is known as the "acid-catalyzed" pathway. However, in neutral and basic solutions (or under a majority of physiological conditions), the dominant reaction pathway is the so-called "base-catalyzed" hydrolysis, e.g., the nucleophilic attack of a hydroxide ion at the carbonyl carbon,[2,3,11] although the neutral hydrolysis (i.e., the direct reaction of amide with a water molecule) can play a nonnegligible role.[18,19] In addition, base-catalyzed hydrolysis of amides has been considered an important reaction model for the enzymatic cleavage of peptide bonds.[20] Thus, the base-catalyzed hydrolysis of amide is more interesting for most of practical reaction conditions such as living systems.

The base-catalyzed hydrolysis of amide is believed to include two major reaction steps.[21] The first step is formation of an anionic tetrahedral intermediate. The second step is decomposition of the intermediate to the hydrolysis products, i.e., carboxylate ion and amine. The heavy-atom isotope effects on the based-catalyzed hydrolysis of formamide reported by Marlier et al.[6] indicate that the formation of the tetrahedral intermediate is rate-determining. On the basis of their observed kinetic isotope effects, Marlier et al.[6] also suggested that one of the water molecules hydrating the hydroxide ion is the actual nucleophile instead of the hydroxide ion itself. In other words, these researchers suggested a general base-catalyzed hydrolysis mechanism. However, using an NMR technique, Slebocka-Tilk et al.[7] recently carried out a proton inventory study on the rates of base-catalyzed hydrolysis of formamide in aqueous solution and found that both nucleophilic and general base mechanisms can be accommodated, but the preferred mechanism is a nucleophilic one proceeding through a transition state having two solvating water molecules remaining on the attacking hydroxide and three additional water molecules attached to the developing amide hydrate oxyanion. The nucleophilic mechanism refers to the specific base-catalyzed hydrolysis, and the specific base is a hydroxide ion, i.e., the hydroxide ion-catalyzed hydrolysis. In the general base mechanism, a water molecule directly attacks the carbonyl carbon of amide and the hydroxide ion acts as a general base.[7]

A full understanding of the detailed reaction mechanisms for amide hydrolysis requires computational studies on the reaction coordinates, in addition to experimental studies. Extensive computational studies have been reported on the mechanisms of the spontaneous hydrolysis (i.e., direct reaction of an amide

* To whom correspondence should be addressed. Telephone: 859-323-3943. Fax: 859-323-3575. E-mail: zhan@uky.edu.

Transition State for Hydrolysis of Amides

J. Phys. Chem. A, Vol. 110, No. 46, 2006 **12645**

with a water molecule)[22–24] and acid-catalyzed hydrolysis.[8,9,12,13,25–27] Computational modeling has also been performed to study base-catalyzed amide hydrolysis pathway and provided some valuable mechanistic insights.[3,8,10,14–16,18,28–35] In general, these computational studies (on the base-catalyzed reaction in both gas phase and solution) have qualitatively demonstrated that solvent effects play a key role in the hydrolysis process; the reaction is very exothermic in the gas phase and involves only moderate energy barriers for all of the reaction steps, whereas aqueous solvent induces a significant energy barrier toward formation of the intermediate. Interestingly, Pliego[16] recently employed a cluster-continuum model to study the possible two reaction pathways of base-catalyzed hydrolysis of formamide: the general base-catalyzed hydrolysis and hydroxide ion-catalyzed hydrolysis. Two or three explicit water molecules solvating the hydroxide ion were included in the reaction coordinate calculations. Through the reaction coordinate calculations, Pliego[16] suggested that the general base-catalyzed hydrolysis pathway does not take place at all and the actual reaction pathway is the direct nucleophilic attack of the hydroxide ion at the carbonyl carbon. Pliego's suggestion is supported by the more recently reported Car-Parrinello molecular dynaimcs (CPMD) simulations.[34] Based on Pliego's suggestion and the insight from the latest CPMD simulations, further mechanistic studies on base-catalyzed hydrolysis of amides should be focused on the formation of the tetrahedral intermediate (i.e., the rate-determining step) of hydroxide ion-catalyzed reaction mechanism.

However, the majority of the computational studies on hydroxide ion-catalyzed amide hydrolysis have been limited to only the smallest amide, i.e., formamide, and the substituent effects on the reaction pathway and free energy barriers of the amide hydrolysis have not been examined computationally. It is unknown whether the observed substituent effects on the free energy barrier of the amide hydrolysis can be reproduced by computational modeling or not. Generally speaking, a mechanistic insight obtained from reaction coordinate calculations on a chemical reaction is reliable only when the calculated results can be used to consistently interpret all of the available experimental observations.

To better understand the reaction mechanism of base-catalyzed amide hydrolysis, here we report a detailed first-principles computational study on the transition-state structures and the corresponding free energy barriers for the formation of the tetrahedral intermediate during hydroxide ion-catalyzed hydrolysis of a series of representative amides. Our first-principles electronic structure calculations account for the possible direct involvement of solvent water molecules in the reaction process.

Computational Methods

The computational strategy used in this study is a hybrid supermolecule-continuum approach,[36] i.e., performing a self-consistent reaction field (SCRF) calculation on a super-molecular solute, based on our recently developed surface and volume polarization for electrostatic interaction (SVPE) implementation.[37–40] Our general approach of the hybrid supermolecule-continuum calculation has been described elsewhere in detail.[36,41–44] The physical meaning of such a hybrid supermolecule-continuum approach is that part of the solvent surrounding the solute is treated quantum mechanically and the remaining bulk solvent is approximated as a polarizable dielectric continuum medium treated by using the SVPE method.[36] The SVPE is also known as the fully polarizable continuum model (FPCM)[45–50] because it fully accounts for both surface and volume polarization effects in the SCRF calculation. In other SCRF implementations, volume polarization effects are ignored or approximately modeled by modifying the surface polarization charge distribution through a simulation and/or charge renormalization,[51–60] or the solute charge distribution is simply represented by a set of point charges at the solute nuclei.[61,62] By performing the hybrid supermolecule-continuum calculations, the more solvent molecules treated quantum mechanically, the better the calculated results. Thus, the calculated results can be improved systematically by increasing the number of explicitly considered solvent molecules in the supermolecular solute, as demonstrated in our previously FPCM-based computational studies.[41–44]

To carry out the free energy calculations using the SVPE-based hybrid supermolecule-continuum approach, we first needed to optimize geometries of all supermolecular solutes. Density functional theory (DFT) with Becke's three-parameter hybrid exchange functional and the Lee–Yang–Parr correlation functional (B3LYP)[63–65] in combination with the 6-31+G(d) basis set was used to fully optimize the geometries of all solutes and supermolecular solutes involved in this study. Vibrational frequency calculations were carried out to confirm the transition states and local minima obtained and to determine the zero-point vibrational energies and thermal corrections to the Gibbs free energies. We note that the free energy corrections based on the harmonic vibrational analysis could produce a very large error in the calculation of the absolute entropy for each molecular species. The harmonic approximation is bad particularly for the normal vibration modes with low frequencies.[42] The more water molecules are explicitly included in the calculation, the larger the possible calculation error will be. Thus, anharmonic corrections are necessary for calculating the absolute entropy. However, as discussed in our previously reported other hybrid supermolecule-continuum calculations,[42] anharmonic corrections to the free energy changes should approximately cancel as there are comparable numbers of low-frequency modes in the reactants, transition states, and intermediates. In addition, intrinsic reaction coordinate (IRC)[66] calculations were performed at the B3LYP/6-31+G(d) level to verify the expected connections of the first-order saddle points with the local minima found on the potential energy surface.

Previous theoretical studies[36,67] of reaction pathways for alkaline ester hydrolyses indicate that electron correlation effects are not important in the geometry optimizations and in calculations of solvent shifts, but are important in final energy calculations in the gas phase, for studying energy profiles of those organic reactions. Thus, the geometries optimized at the B3LYP/6-31+G(d) level were employed to perform single-point energy calculations at higher levels, including the MP2/6-31+G-(d), MP2/aug-cc-pVDZ, MP2/aug-cc-pVTZ, and CCSD(T)/aug-cc-pVDZ, in the gas phase.

The bulk solvent shifts of the free energy barriers were evaluated by performing SVPE calculations at the HF/6-31+G-(d) level on the solutes and supermolecular solutes with the geometries optimized at the B3LYP/6-31+G(d) level. Some SVPE calculations were also performed at the HF/6-31++G-(d,p) level for the hydrolysis of formamide to confirm that the 6-31+G(d) basis set is sufficiently large for the SVPE calculations. Because the solute cavity surface is defined as a solute electron charge isodensity contour determined self-consistently during the SVPE iteration process, the SVPE results, converged to the exact solution of Poisson's equation with a given numerical tolerance,[37] depend only on the contour value at a given dielectric constant and on the quantum chemical approach
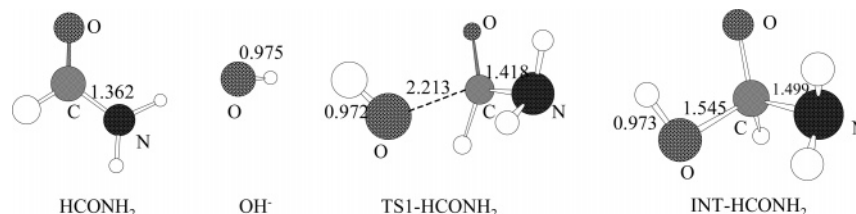
Figure 1. Geometries of the reactants, transition state, and tetrahedral intermediate optimized at the B3LYP/6-31+G(d) level for the formation of the tetrahedral intermediate without including any explicit water molecule in the reaction system.

TABLE 1: Calculated Gibbs Free Energy Barriers (kcal/mol) for the Formation of the Tetrahedral Intermediate during Hydroxide Ion-Catalyzed Hydrolysis of Formamide (FA) in Aqueous Solution in Comparison with Available Experimental Value[a]

Method[b]	FA + OH$^-$ [c]	FA(H$_2$O) + OH$^-$(H$_2$O)$_3$ [d]	FA(H$_2$O)$_2$ + OH$^-$(H$_2$O)$_3$ [e]	FA(H$_2$O)$_3$ + OH$^-$(H$_2$O)$_3$ [f]
MP2/6-31+G(d)	16.8	24.6	21.9(22.0)	22.1
MP2/aug-cc-pVDZ	15.8	25.2	23.3(23.4)	23.5
MP2/aug-cc-pVTZ	17.2	26.0	23.9(24.0)	24.2
CCSD(T)/aug-cc-pVDZ	14.2	23.8	21.6(21.7)	21.7
expt[f]			21.2	

[a] All energetic values are given for the usual standard reference state (1 mol/L for all of the molecular species in solution at $T = 298.15$ K). [b] All energy calculations were performed by using geometries optimized at the B3LYP/6-31+G(d) level. Zero-point vibration and thermal corrections were evaluated at the B3LYP/6-31+G(d) level. Indicated in the table are the methods for the energy calculations neglecting the bulk solvent effects. Unless indicated otherwise, the bulk solvent shifts were determined by carrying out the SVPE calculations at the HF/6-31+G(d) level. For the values in parentheses, the bulk solvent shifts were determined by carrying out the SVPE calculations at the HF/6-31++G(d,p) level, instead of the HF/6-31+G(d) level. [c] No explicit solvent water molecule was included in the calculations; the entire solvent was considered as a fully polarizable continuum medium. [d] Four explicit solvent water molecules were included in the calculations; the remaining bulk solvent was considered as a fully polarizable continuum medium. [e] Five explicit solvent water molecules were included in the calculations; the remaining bulk solvent was considered as a fully polarizable continuum medium. [f] Six explicit solvent water molecules were included in the calculations; the remaining bulk solvent was considered as a fully polarizable continuum medium. [f] Experimental free energy barrier from ref 18.

that has been used. A single parameter value of 0.001 au has been determined on the basis of an extensive calibration study[38] using the experimental conformational free energy differences (62 experimental observations) of various polar solutes in various solvents. Based on the fitting process employed in the calibration, the root-mean-squares (rms) deviation of the 62 experimental values from the results calculated by SVPE method using the 0.001 au contour is 0.096 kcal/mol.[38] The SVPE procedure using the 0.001 au contour has been shown to be reliable for evaluating the bulk solvent effects.[36,41-50] Thus, the 0.001 au contour was used for all the SVPE calculations in this study. It has also been shown[36,41-44] that the solvent shifts determined by the SVPE calculations are rather insensitive to the electron correlation level and basis set used; for example, there is little difference between the results of the SVPE calculations at the HF/6-31++G(d,p) and MP2/6-31++G(d,p) levels.

The free energy barrier for a reaction step in aqueous solution was taken as a sum of the free energy change calculated at the CCSD(T)/aug-cc-pVDZ//B3LYP/6-31+G(d) level neglecting bulk solvent effects and the corresponding bulk solvent shift determined by the SVPE calculations at the HF/6-31+G(d) level. To appropriately compare the calculated results with available experimental free energy barriers,[1,18] the calculated Gibbs free energies of all molecular species were corrected to be consistent with the standard reference state of the solution, i.e., the solute concentration of 1 mol/L at $T = 298.15$ K.

The computer codes used to carry out the computations are Gaussian03 program[68] for the B3LYP/6-31+G(d) and MP2/6-31+G(d) calculations, NWChem program[69] for the other MP2 and CCSD(T) calculations, and a local version[37] of the GAMESS program[70] for all of the SVPE calculations. The computers used to perform the calculations are HP's Superdome supercomputer (a shared-memory system with 256 processors) at the University of Kentucky Center for Computational Sciences, HP's Itanium2 1980-processors Linux cluster at the

Environmental Molecular Science Laboratory (EMSL) of Pacific Northwest National Laboratory (PNNL), and IBM ×335 34-processors Linux cluster and SGI multiprocessors Origin computers in our own laboratory.

Results and Discussion

Optimized Transition-State Structure and Calculated Free Energy Barrier for the Hydrolysis of Formamide. First of all, our reaction coordinate calculation was performed first on hydroxide ion-catalyzed hydrolysis of formamide (i.e., HCONH$_2$) without explicitly including water molecules in the reaction process. The reaction coordinate calculation was followed by single-point energy calculations that implicitly account for the solvent effects with the SVPE method. Figure 1 depicts the optimized geometries of the reactants, transition state, and intermediate. As seen in Figure 1, the reaction starts from the hydroxide ion attack at the carbonyl carbon of formamide to form the tetrahedral intermediate INT-HCONH$_2$ via the first transition state TS1-HCONH$_2$. As one can see in Table 1, without explicitly including any water molecule in the reaction coordinate calculation, the free energy barrier values calculated at all levels are significantly lower than the experimental value (21.2 kcal/mol).[18]

To examine the effects of solvent water molecules on the reaction process, we further carried out reaction coordinate calculations on the reaction system with four explicit water molecules. As depicted in Figure 2, we found two transition-state structures, i.e., TS1-HCONH$_2$(H$_2$O)$_4$-a and TS1-HCONH$_2$-(H$_2$O)$_4$-b, for the formation of the tetrahedral intermediate. In the optimized TS1-HCONH$_2$(H$_2$O)$_4$-a structure, two water molecules have hydrogen bonds with the hydroxide oxygen, while the other two water molecules have hydrogen bonds with the carbonyl oxygen of the amide. In the optimized TS1-HCONH$_2$(H$_2$O)$_4$-b structure, the hydroxide oxygen also hydrogen-bonds with two water molecules, but the carbonyl oxygen

Transition State for Hydrolysis of Amides

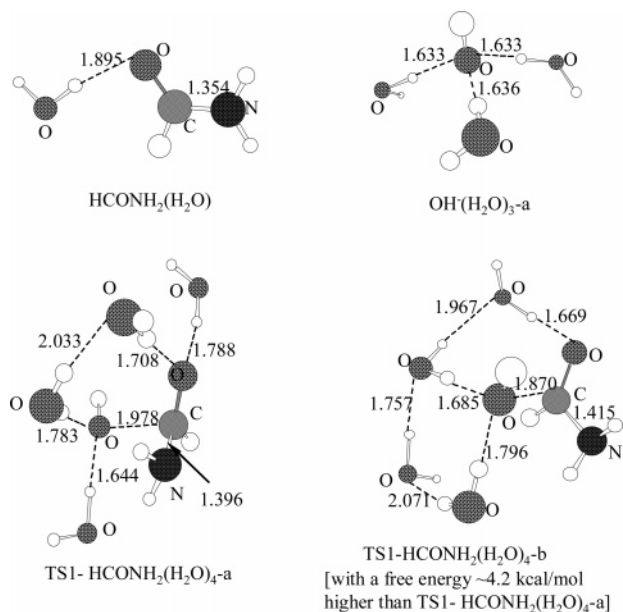*J. Phys. Chem. A, Vol. 110, No. 46, 2006* **12647**

Figure 2. Geometries of the reactants and transition state for the formation of the tetrahedral intermediate optimized at the B3LYP/6-31+G(d) level for hydroxide ion-catalyzed hydrolysis of formamide with four explicit water molecules included in the reaction system. The relative free energies of the transition-state structures were determined by the gas-phase energy calculations at the CCSD(T)/aug-cc-pVDZ level; the zero-point vibration, thermal corrections, and solvent shifts were determined in the way described in the text.

Figure 3. Geometries of the reactant and transition state for the formation of the tetrahedral intermediate optimized at the B3LYP/6-31+G(d) level for hydroxide ion-catalyzed hydrolysis of formamide with five explicit water molecules included in the reaction system. The relative free energies of the transition-state structures were determined by the gas-phase energy calculations at the CCSD(T)/aug-cc-pVDZ level; the zero-point vibration, thermal corrections, and solvent shifts were determined in the way described in the text.

hydrogen-bonds with only one water molecule; the fourth water molecule hydrogen-bonds with the two water molecules that have hydrogen bonds with the hydroxide oxygen. The calculated Gibbs free energy of the TS1-HCONH$_2$(H$_2$O)$_4$-b structure is 4.2 kcal/mol higher than that of the TS1-HCONH$_2$(H$_2$O)$_4$-a structure when $T = 298.15$ K, indicating that the solute−solvent hydrogen bonding is stronger than the solvent−solvent hydrogen bonding for this particular system. Starting from the lowest-free-energy structure TS1-HCONH$_2$(H$_2$O)$_4$-a, the IRC calculation in the forward reaction direction went to a tetrahedral intermediate (INT), whereas the IRC calculation in the reverse reaction direction pointed to the separated reactants HCONH$_2$-(H$_2$O) and HO$^-$(H$_2$O)$_3$ shown in Figure 2. In comparison of the TS1-HCONH$_2$(H$_2$O)$_4$ structures depicted in Figure 2 with the TS1-HCONH$_2$ structure depicted in Figure 1, we note that except for the hydrogen bonding to water, there is little difference between the tetrahedral intermediate formation of the hydrolysis for the supermolecular reaction system and that of the hydrolysis in the water-free gas phase. Ignoring the solvent water molecules, the geometries of TS1-HCONH$_2$(H$_2$O)$_4$ in Figure 2 are very similar to the corresponding geometry of TS1-HCONH$_2$ in Figure 1. We may conclude that the solvation within our consideration does not change the reaction pathway for the tetrahedral intermediate formation of the hydrolysis as no solvent molecule is directly involved in the change of covalent bonds. As one can see from Table 1, the free energy barrier (23.8 kcal/mol) calculated at the CCSD(T)/aug-cc-pVDZ level is only 2.6 kcal/mol higher than the experimental free energy barrier (21.2 kcal/mol)[18] for the base-catalyzed hydrolysis of formamide.

To further improve the quantitative description of the free energy barrier for the formation of the tetrahedral intermediate, we also performed reaction coordinate calculations with five and six explicit water molecules. We tested this using various initial structures in the reaction coordinate calculations. With five explicit water molecules, each initial structure used to
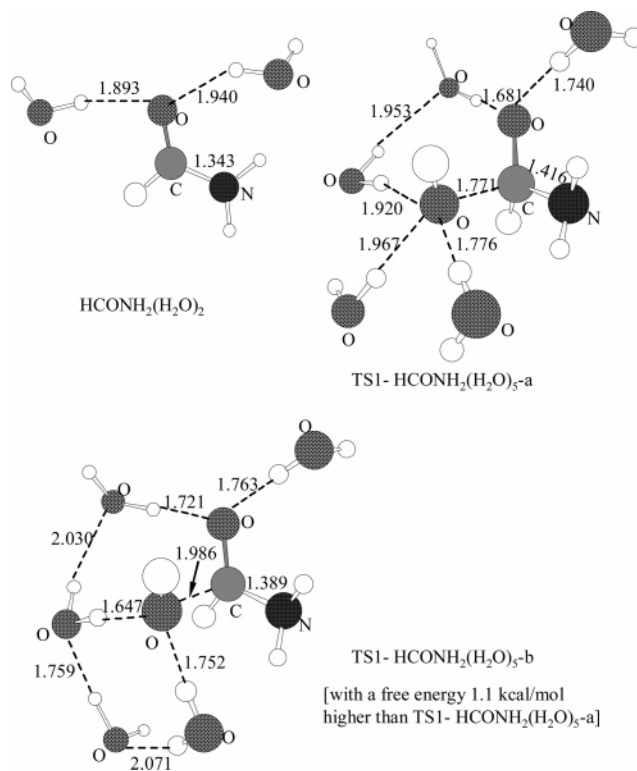
optimize geometry of the transition state was constructed from the optimized TS1-HCONH$_2$(H$_2$O)$_4$-a geometry by adding a fifth water molecule. It appears that the fifth water molecule may hydrogen-bond with the hydroxide oxygen, with the carbonyl oxygen of the amide, or with some of the first four water molecules. By testing all of these possibilities, we only found two first-order saddle points on the potential energy surface. Depicted in Figure 3 are the optimized two transition-state structures, i.e., TS1-HCONH$_2$(H$_2$O)$_5$-a and TS1-HCONH$_2$-(H$_2$O)$_5$-b, associated with these two saddle points. Of these transition-state structures, TS1-HCONH$_2$(H$_2$O)$_5$-a has the lowest free energy in aqueous solution as indicated in Figure 3. In the TS1-HCONH$_2$(H$_2$O)$_5$-a structure optimized, the fifth water molecule hydrogen-bonds with the hydroxide oxygen. Starting from the TS1-HCONH$_2$(H$_2$O)$_5$-a structure, the IRC calculation in the reverse direction clearly pointed to the separated reactants HO$^-$(H$_2$O)$_3$ and HCONH$_2$(H$_2$O)$_2$ (depicted in Figure 3), whereas the IRC calculation in the forward direction went to an expected tetrahedral intermediate (not shown). By using the optimized geometries of HO$^-$(H$_2$O)$_3$, HCONH$_2$(H$_2$O)$_2$, and TS1-HCONH$_2$-(H$_2$O)$_5$-a, the free energy barrier of 21.6 kcal/mol (or 21.7 kcal/mol; see Table 1) calculated at the CCSD(T)/aug-cc-pVDZ level is in good agreement with the experimental free energy barrier of 21.2 kcal/mol.[18]

Similarly, with six explicit water molecules, we tested a variety of possible TS1-HCONH$_2$(H$_2$O)$_6$ structures and found four stable structures depicted in Figure 4. The TS1-HCONH$_2$-(H$_2$O)$_6$-a structure has the lowest free energy in comparison with the other TS1-HCONH$_2$(H$_2$O)$_6$ structures. Based on this transition-state structure, the free energy barrier was calculated to be 21.7 kcal/mol on the basis of the calculations at the CCSD-
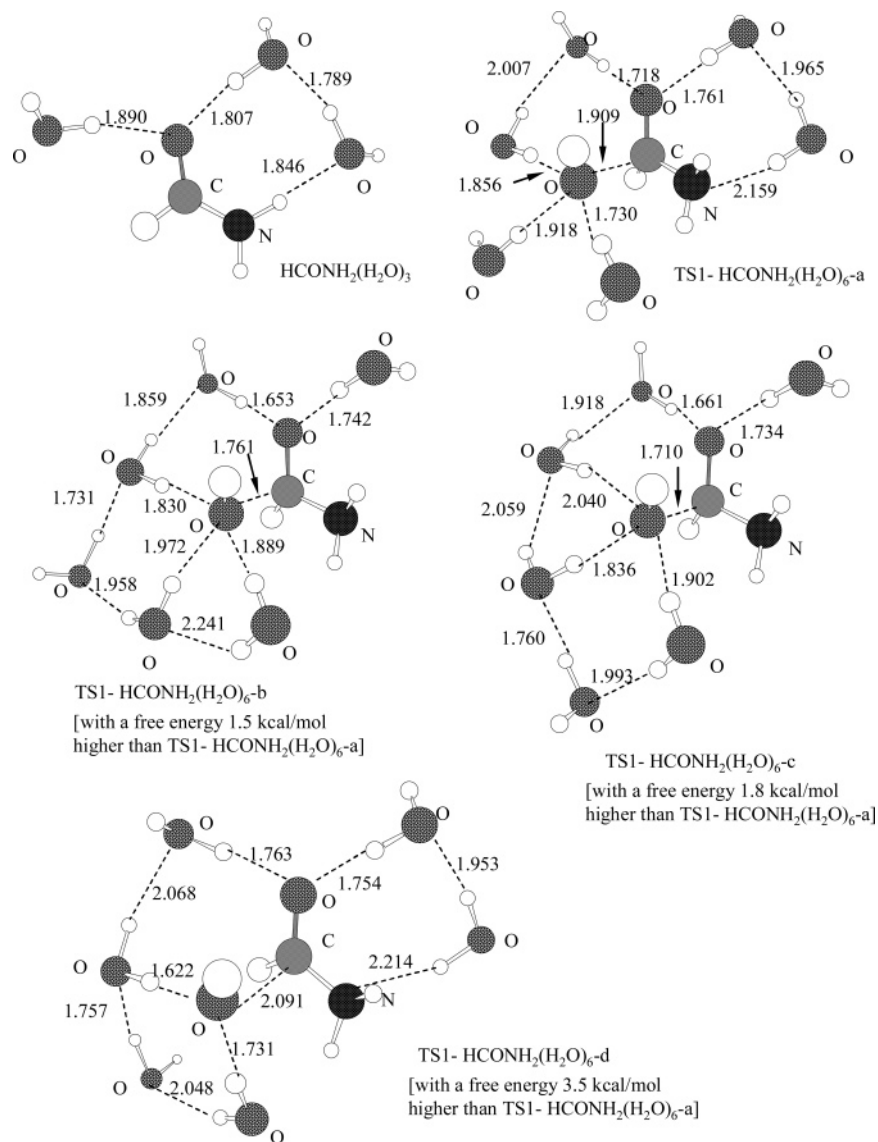
Figure 4. Geometries of the reactant and transition state for the formation of the tetrahedral intermediate optimized at the B3LYP/6-31+G(d) level for hydroxide ion-catalyzed hydrolysis of formamide with six explicit water molecules included in the reaction system. The relative free energies of the transition-state structures were determined by the gas-phase energy calculations at the CCSD(T)/aug-cc-pVDZ level; the zero-point vibration, thermal corrections, and solvent shifts were determined in the way described in the text.

(T)/aug-cc-pVDZ level. The free energy barrier calculated with six explicit water molecules at the CCSD(T)/aug-cc-pVDZ level is only 0.1 kcal/mol higher than that calculated with five explicit water molecules at the same level. For this reason, we only considered five explicit water molecules for the hydrolysis of other amides (see below).

In comparison with previously reported computational studies on the hydrolysis of formamide, we note that our optimized most favorable transition-state structure, i.e., TS1-HCONH$_2$-(H$_2$O)$_5$-a depicted in Figure 3 or TS1-HCONH$_2$(H$_2$O)$_6$-a depicted in Figure 4, is qualitatively consistent with that obtained from the multiple-steering ab initio molecular dynamics simulations reported by Carloni and co-workers.[32] Their multiple-steering ab initio molecular dynamics simulations using CPMD approach (with BLYP functional) also led to a transition-state structure with three water molecules remaining on the attacking hydroxide. Most recently reported ab initio metadynamics simulations (also using CPMD approach with the BLYP functional) reported by Klein and co-workers[34] suggested only two water molecules remaining on the attacking hydroxide. Nevertheless, their CPMD simulations were mainly focused on

the mechanistic question of whether the base-catalyzed hydrolysis of formamide should follow the general-base mechanism or direct nucleophilic attack mechanism. Compared to these CPMD simulations, our current computational approach has both disadvantages and advantages. The main disadvantage is that the reaction dynamics was not examined; we were able to examine only the possible transition-state structures and the corresponding reactant structures. The main advantage is that our first-principles electronic structures calculations on the reaction center were performed at the higher electron-correlation levels, i.e., MP2 and CCSD(T). As depicted in Figure 3, the Gibbs free energy of the TS1-HCONH$_2$(H$_2$O)$_5$-b structure calculated at the CCSD(T)/aug-cc-pVDZ level is 1.1 kcal/mol higher than that of the TS1-HCONH$_2$(H$_2$O)$_5$-a structure. All of the MP2 energy calculations are also qualitatively consistent with the relative Gibbs free energies calculated at the CCSD-(T)/aug-cc-pVDZ level. However, when the energies calculated at the CCSD(T)/aug-cc-pVDZ level were all replaced by the corresponding energies calculated at the B3LYP/6-31+G(d) and BLYP/6-31+G(d) levels, the calculated Gibbs free energy of the TS1-HCONH$_2$(H$_2$O)$_5$-b structure became lower than that

Transition State for Hydrolysis of Amides

J. Phys. Chem. A, Vol. 110, No. 46, 2006 **12649**

of the TS1-HCONH$_2$(H$_2$O)$_5$-a structure by 0.7 and 2.0 kcal/mol, respectively. So, the DFT and CCSD(T) (or MP2) calculations led to qualitatively different relative Gibbs free energies of the transition-state structures TS1-HCONH$_2$(H$_2$O)$_5$-a (with three water molecules remaining on the attacking hydroxide) and TS1-HCONH$_2$(H$_2$O)$_5$-b (with two water molecules remaining on the attacking hydroxide). Therefore, computational modeling at a sufficiently high level is necessary to theoretically determine the number of water molecules remaining on the attacking hydroxide in the transition state. An ideal computational approach would be to perform ab initio metadynamics simulations at the CCSD(T) or MP2 level in the future.

Comparison with Kinetic Proton Inventory Data for Available Hydrolysis of Formamide. The reaction coordinate calculations discussed above reveal that the hydroxide oxygen and carbonyl oxygen of formamide together have hydrogen bonds with a total of five water molecules in the most favorable transition-state structure, i.e., TS1-HCONH$_2$(H$_2$O)$_5$-a depicted in Figure 3 or TS1-HCONH$_2$(H$_2$O)$_6$-a depicted in Figure 4. The most favorable transition-state structure determined by the first-principles reaction coordinate calculations is consistent with the proton inventory data reported by Slebocka-Tilk et al.,[7] when we are only concerned with the total number of water molecules hydrogen-bonding with the hydroxide oxygen and carbonyl oxygen in the transition state. However, a notable difference between the optimized TS1-HCONH$_2$(H$_2$O)$_5$-a geometry and the reported proton inventory analysis exists in the structural detail of the transition state. Slebocka-Tilk et al.[7] concluded that, in the preferred nucleophilic mechanism, the transition state has two solvating water molecules remaining on the attacking hydroxide and three additional water molecules attached to the developing amide hydrate oxyanion (i.e. the carbonyl oxygen of formamide), whereas our optimized TS1-HCONH$_2$(H$_2$O)$_5$-a geometry has three solvating water molecules remaining on the attacking hydroxide and two additional water molecules attached to the carbonyl oxygen of formamide.

To understand this discrepancy between our optimized transition-state geometry and the proton inventory analysis, we carefully reexamined the proton inventory analysis reported by Slebocka-Tilk et al.[7] and noted that Slebocka-Tilk et al. only considered two mechanistic possibilities for hydroxide ion-catalyzed hydrolysis of formamide: one was through a transition state having two solvating water molecules remaining on the attacking hydroxide and three additional water molecules attached to the carbonyl oxygen of formamide; the other was a minimal nucleophilic mechanism through a transition state having two solvating water molecules remaining on the attacking hydroxide and without any water molecule attached to the carbonyl oxygen of formamide. The former mechanistic possibility was represented by the following equation:[7]

$$k_n = k_0(1 - n + 1.22^{(1-x)}n)(1 - n + 0.7^{(1-x)}n)^2(1 - n + 0.7^y n)^3/(1 - n + 1.22n)(1 - n + 0.7n)^3 \quad (1)$$

where k_n is the second-order rate constant for base-catalyzed hydrolysis of formamide in aqueous media of different molar fraction (n), x is a parameter describing the structure of the transition state in terms of its progress from reactants ($x = 0$) to the intermediate ($x = 1$), and y is an independent parameter representing progress of the solvation change on the developing oxyanion (i.e., the carbonyl oxygen of formamide). The x value was believed to be ≥0.5 on the basis of Kirsch's experimental results for the kinetic isotope effects.[71] Assuming $x = 0.5-0.9$,

TABLE 2: Summary of the Results Obtained from the Nonlinear Least-Squares (NLLSQ) Fitting of the Original Proton Inventory Data Reported in Reference 7 According to Equations 1 and 2

X	k_0 (M^{-1} s^{-1})	$\phi_1{}^a$	$\phi_2{}^b$	$\phi_4{}^c$	RMSD (M^{-1} s^{-1})^d
		According to Equation 1			
0.9	3.23 × 10^{-3}	1.02	0.96	0.83	0.078 × 10^{-3}
0.8	3.23 × 10^{-3}	1.04	0.93	0.85	0.079 × 10^{-3}
0.7	3.23 × 10^{-3}	1.06	0.90	0.86	0.079 × 10^{-3}
0.6	3.23 × 10^{-3}	1.08	0.87	0.88	0.079 × 10^{-3}
0.5	3.22 × 10^{-3}	1.10	0.84	0.89	0.077 × 10^{-3}
		According to Equation 2			
0.9	3.22 × 10^{-3}	1.02	0.96	0.77	0.074 × 10^{-3}
0.8	3.23 × 10^{-3}	1.04	0.93	0.81	0.077 × 10^{-3}
0.7	3.23 × 10^{-3}	1.06	0.90	0.84	0.079 × 10^{-3}
0.6	3.23 × 10^{-3}	1.08	0.87	0.88	0.079 × 10^{-3}
0.5	3.22 × 10^{-3}	1.10	0.84	0.92	0.076 × 10^{-3}

^{a} Calculated as $\phi_1 = (1.22)^{1-x}$. ^{b} Calculated as $\phi_2 = (0.7)^{1-x}$. ^{c} Calculated as $\phi_4 = (0.7)^y$. ^{d} The root-mean-square-deviation (RMSD) of the k_n values determined by the fitted equation to the corresponding experimental k_n values.[7]

Slebocka-Tilk et al.[7] found that the proton inventory data fit eq 1 well, suggesting that the mechanism associated with eq 1 is possible.

The question is whether the proton inventory data[7] can also satisfactorily fit another equation associated with a slightly different mechanism. Their proton inventory analysis[7] actually does not rule out any other mechanistic possibility which has not been examined yet. Following the general strategy of the proton inventory analysis described by Slebocka-Tilk et al.,[7] we can have the following equation based on the most favorable structure TS1-HCONH$_2$(H$_2$O)$_5$-a of the transition state for the rate-determining step of hydroxide ion-catalyzed hydrolysis of formamide, if our conclusion obtained from the reaction coordinate calculations is correct:

$$k_n = k_0(1 - n + 1.22^{(1-x)}n)(1 - n + 0.7^{(1-x)}n)^3(1 - n + 0.7^y n)^2/(1 - n + 1.22n)(1 - n + 0.7n)^3 \quad (2)$$

We carried out the nonlinear least squares (NLLSQ) fitting of the original proton inventory data reported by Slebocka-Tilk et al.[7] to eq 2. For comparison, we also performed the NLLSQ fitting of the same proton inventory data to eq 1. The NLLSQ fitting results are summarized in Table 2. The results (including all of the k_0, x, ϕ_1, ϕ_2, and ϕ_4 values) of the NLLSQ fitting to eq 1 are identical to what was reported by Slebocka-Tilk et al.,[7] showing that our NLLSQ fitting procedure is consistent with that used by Slebocka-Tilk et al. The quality of the NLLSQ fit of the original proton inventory data to an empirical equation is related to the root-mean-square-deviation (RMSD) of the k_n values determined by the fitted equation to the corresponding experimental k_n values. The smaller the RMSD value, the better the fit. The data summarized in Table 2 clearly reveal that the proton inventory data can also fit eq 2 satisfactorily. When $x = 0.5-0.9$, the RMSD values (~(0.074−0.079) × 10^{-3} M^{-1} s^{-1}) associated with eqs 1 and 2 are all very close to the RMSD value of 0.059 × 10^{-3} M^{-1} s^{-1} (calculated with the deviations of the original experimental errors reported for all of the k_n values[7]). The RMSD values associated with eq 2 are always slightly smaller than or equal to the corresponding RMSD values associated with eq 1. Even if neglecting the slight difference between the two sets of RMSD values, we at least can conclude that the proton inventory data[7] fit both eqs 1 and 2 satisfactorily. So, the original proton inventory data[7] cannot distinguish the two mechanistic possibilities associated with eqs 1 and 2. Taking

CH₃CONH(CH₃)(H₂O)₂   TS1-CH₃CONH(CH₃)(H₂O)₅-b

TS1-CH₃CONH(CH₃)(H₂O)₅-a
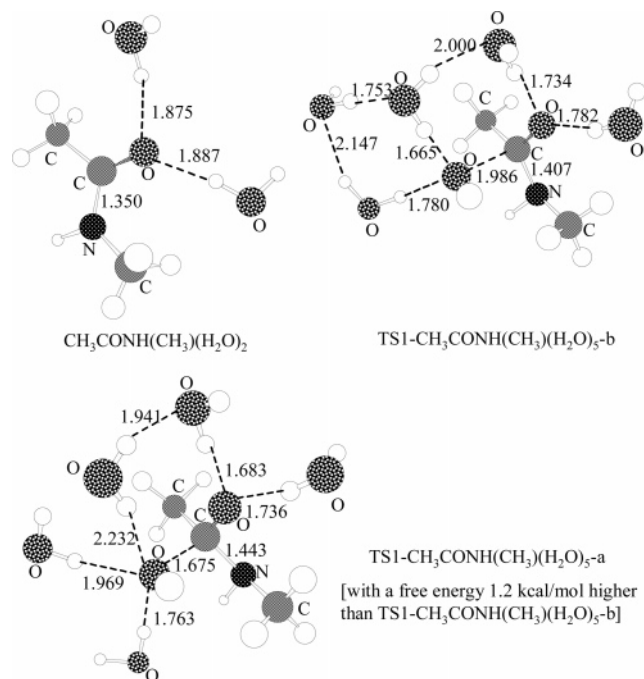[with a free energy 1.2 kcal/mol higher than TS1-CH₃CONH(CH₃)(H₂O)₅-b]

Figure 5. Geometries of the reactant and transition state for the formation of the tetrahedral intermediate optimized at the B3LYP/6-31+G(d) level for hydroxide ion-catalyzed hydrolysis of *N*-methylacetamide with five explicit water molecules included in the reaction system. The relative free energies of the transition-state structures were determined by the gas-phase energy calculations at the CCSD(T)/aug-cc-pVDZ level; the zero-point vibration, thermal corrections, and solvent shifts were determined in the way described in the text.

this new analysis of the proton inventory data together with our reaction coordinate calculations, we may further conclude that the transition-state structure for the rate-determining step of hydroxide ion-catalyzed hydrolysis of formamide should have three (rather than two) solvating water molecules remaining on the attacking hydroxide oxygen and two (rather than three) additional water molecules attached to the carbonyl oxygen of formamide.

Transition-State Structures and Free Energy Barriers for the Hydrolysis of Other Amides. To explore the substituent effects on the transition-state structures and the free energy barriers, we also examined the first reaction step of hydroxide ion-catalyzed hydrolysis of three other representative amides, including *N*-methylacetamide (i.e., CH₃CONHCH₃), *N,N*-dimethylformamide (DMF, i.e., HCON(CH₃)₂), and *N,N*-dimethylacetamide (DMA, i.e., CH₃CON(CH₃)₂). For each reaction system, five explicit water molecules were included in the reaction coordinate calculations. The optimized geometries are depicted in Figures 5−7. As seen in Figure 5, the reaction coordinate calculations revealed two transition-state structures, TS1-CH₃CONHCH₃(H₂O)₅-a and TS1-CH₃CONHCH₃(H₂O)₅-b, for the first reaction step. The TS1-CH₃CONHCH₃(H₂O)₅-a and TS1-CH₃CONHCH₃(H₂O)₅-b structures are similar to the TS1-HCONH₂(H₂O)₅-a and TS1-HCONH₂(H₂O)₅-b structures, respectively, in terms of the numbers of hydrogen bonds with both the hydroxide oxygen and the carbonyl oxygen of the amide. Similar results were also obtained for the hydrolysis of DMA, as shown in Figure 7. However, the overall strength of the three hydrogen bonds with the hydroxide oxygen in the TS1-CH₃CONHCH₃(H₂O)₅-a or TS1-DMA(H₂O)₅-a structure is expected to be significantly weaker than that of the corresponding three hydrogen bonds in the TS1-HCONH₂(H₂O)₅-a structure, based on the optimized H···O distances shown in Figures 3, 5, and 7. As a result, the TS1-CH₃CONHCH₃(H₂O)₅-b
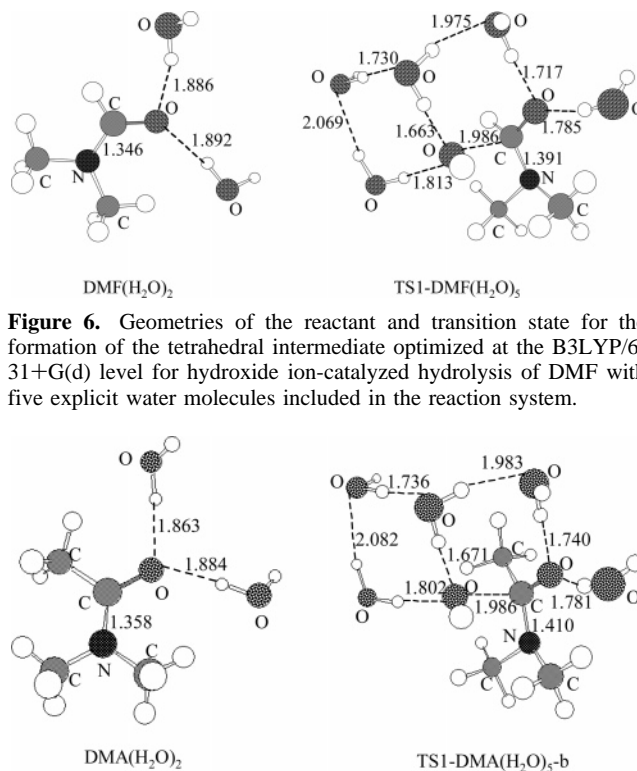

DMF(H₂O)₂   TS1-DMF(H₂O)₅

Figure 6. Geometries of the reactant and transition state for the formation of the tetrahedral intermediate optimized at the B3LYP/6-31+G(d) level for hydroxide ion-catalyzed hydrolysis of DMF with five explicit water molecules included in the reaction system.
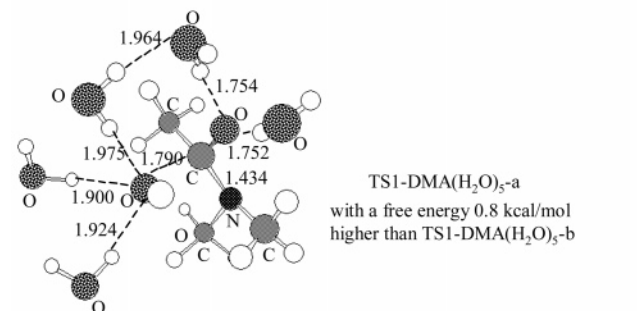

DMA(H₂O)₂   TS1-DMA(H₂O)₅-b

TS1-DMA(H₂O)₅-a
with a free energy 0.8 kcal/mol higher than TS1-DMA(H₂O)₅-b

Figure 7. Geometries of the reactant and transition state for the formation of the tetrahedral intermediate optimized at the B3LYP/6-31+G(d) level for hydroxide ion-catalyzed hydrolysis of DMA with five explicit water molecules included in the reaction system. The relative free energies of the transition-state structures were determined by the gas-phase energy calculations at the CCSD(T)/aug-cc-pVDZ level; the zero-point vibration, thermal corrections, and solvent shifts were determined in the way described in the text.

structure has the lowest free energy for *N*-methylacetamide, and the TS1-DMA(H₂O)₅-b structure has the lowest free energy for DMA. For the hydrolysis of DMF, we only found the transition-state structure, i.e., TS1-DMF(H₂O)₅, which is similar to TS1-HCONH₂(H₂O)₅-b, CH₃CONHCH₃(H₂O)₅-b, and TS1-DMA-(H₂O)₅-b in terms of the numbers of the hydrogen bonds with the hydroxide oxygen and carbonyl oxygen; we did not find another first-order saddle point associated with a transition-state structure similar to TS1-HCONH₂(H₂O)₅-a, CH₃CONHCH₃-(H₂O)₅-a, and TS1-DMA(H₂O)₅-a, although we carefully tested the transition-state geometry optimizations using various initial structures.

According to the optimized lowest-free-energy TS1 structures depicted in Figures 5−7, we can conclude that for hydroxide ion-catalyzed hydrolysis of *N*-methylacetamide, DMF, and DMA, the most favorable rate-determining transition-state structure always has two solvating water molecules remaining on the attacking hydroxide oxygen and two additional water molecules attached to the carbonyl oxygen of the amide. When

Transition State for Hydrolysis of Amides

J. Phys. Chem. A, Vol. 110, No. 46, 2006 **12651**

TABLE 3: Calculated Gibbs Free Energy Barriers (kcal/mol) for the Rate-Determining Step of Hydroxide Ion-Catalyzed Hydrolysis of Formamide, *N*-Methylacetamide, DMF, and DMA in Aqueous Solution in Comparison with Available Experimental Data[a]

method[b]	formamide	*N*-methylacetamide	DMF	DMA
MP2/6-31+G(d)	21.9	22.3	22.5	25.6
MP2/aug-cc-pVDZ	23.3	24.2	24.5	27.5
CCSD(T)/aug-cc-pVDZ	21.6	22.7	23.1	26.0
expt.	21.2 [c]	21.5 [d]	22.6 [e]	24.1 [e]

[a] All energetic values are given for the usual standard reference state (1 mol/L for all molecular species in solution at $T = 298.15$ K). [b] Five explicit solvent water molecules were included in the calculations; the remaining bulk solvent was considered as a fully polarizable continuum medium All energy calculations were performed by using geometries optimized at the B3LYP/6-31+G(d) level. Zero-point vibration and thermal corrections were evaluated at the B3LYP/6-31+G(d) level. Indicated in the table are the methods for the energy calculations neglecting the bulk solvent effects. The bulk solvent shifts were determined by carrying out the SVPE calculations at the HF/6-31+G(d) level. [c] Experimental free energy barrier from ref 18. [d] Experimental free energy barrier from ref 72. [e] Experimental free energy barriers from ref 1.

some or all of the hydrogen atoms of formamide are replaced by methyl groups, the total number of the hydrogen bonds with the hydroxide oxygen in the rate-determining transition state decreases from three for formamide to two for *N*-methylacetamide, DMF, and DMA.

Based on the optimized lowest-free-energy TS1 structures depicted in Figures 3 and 5−7, the free energy barriers calculated with five explicit water molecules at the CCSD(T)/aug-cc-pVDZ level are 21.6, 22.7, 23.1, and 26.0 kcal/mol for formamide, *N*-methylacetamide, DMF, and DMA, respectively (see Table 3). The calculated results clearly show a trend of the substituent shift of the calculated free energy barrier for hydroxide ion-catalyzed hydrolysis of amide (RCONR′R″); i.e., the free energy barrier increases when the bulk sizes of substituents R, R′, and R″ become larger. The larger substituents likely hinder the formation of stronger hydrogen bonding between the attacking hydroxide oxygen and solvent water molecules in the rate-determining transition state and, therefore, destabilize the transition state and increase the free energy barrier. The calculated free energy barriers are in good agreement with available experimental free energy barriers 21.2, 21.5, 22.6, and 24.1 kcal/mol for formamide,[18] *N*-methylacetamide,[72] DMF, and DMA,[1] respectively.

Conclusion

Reaction coordinate calculations based on the first-principles electronic structure approach and hybrid supermolecule-continuum calculations on hydroxide ion-catalyzed hydrolysis of amides have demonstrated that the favorable transition-state structure optimized for the rate-determining step of hydroxide ion-catalyzed hydrolysis of formamide could have three solvating water molecules remaining on the attacking hydroxide oxygen and two additional water molecules attached to the carbonyl oxygen of formamide. The calculated results have also demonstrated that the number of water molecules hydrogen-bonding with the attacking hydroxide in the transition state is affected by the substituent effects. When some or all of the hydrogen atoms of formamide are replaced by methyl groups, the total number of water molecules hydrogen-bonding with the attacking hydroxide in the transition state decreases from three for formamide to two for *N*-methylacetamide, DMF, and DMA. Thus, for hydroxide ion-catalyzed hydrolysis of *N*-methylacetamide, DMF, and DMA, the most favorable transition state only has two solvating water molecules remaining on the attacking hydroxide and two additional water molecules attached to the carbonyl oxygen of the amide. The larger substituents of the amide hinder the solvent water molecules approaching the attacking hydroxide oxygen in the transition state and, therefore, destabilize the transition state and increase the free energy barrier. By using the optimized most favorable transition-state

structures, the calculated free energy barriers, i.e., 21.6 (or 21.7), 22.7, 23.1, and 26.0 kcal/mol for formamide, *N*-methylacetamide, DMF, and DMA, respectively, are in good agreement with the available experimental free energy barriers, i.e. 21.2, 21.5, 22.6, and 24.1 kcal/mol for formamide, *N*-methylacetamide, DMF, and DMA, respectively.

References and Notes

(1) Guthrie, J. P. *J. Am. Chem. Soc.* **1974**, *96*, 3608.

(2) Hine, J.; King, R. S.-M.; Midden, W. R.; Sinha, A. *J. Org. Chem.* **198**1, *46*, 3186.

(3) Robinson, B. A.; Tester, J. W. *Int. J. Chem. Kinet.* **1990**, *22*, 431.

(4) Slebocka-Tilk, H.; Bennet, A. J.; Hogg, H. J.; Brown, R. S. *J. Am. Chem. Soc.* **1991**, *113*, 1288.

(5) Brown, R. S.; Bennet, A. J.; Œlebocka-Tilk, H. *Acc. Chem. Res.* **1992**, *25*, 481.

(6) Marlier, J. F.; Dopke, N. C.; Johnstone, K. R.; Wirdzig, T. J. *J. Am. Chem. Soc.* **1999**, *121*, 4356.

(7) Slebocka-Tilk, H.; Neverov, A. A.; Brown, R. S. *J. Am. Chem. Soc.* **2003**, *125*, 1851.

(8) Krug, J. P.; Popelier, P. L. A.; Bader, R. F. W. *J. Phys. Chem.* **1992**, *96*, 7604.

(9) Antonczak, S.; Ruiz-Lopez, M. F.; Rivail, J. L. *J. Am. Chem. Soc.* **1994**, *116*, 3912.

(10) Stanton, R. V.; Peräkylä, M.; Bakowies, D.; Kollman, P. A. *J. Am. Chem. Soc.* **1998**, *120*, 3448.

(11) Bakowies, D.; Kollman, P. A. *J. Am. Chem. Soc.* **1999**, *121*, 5712.

(12) Zahn, D. *J. Phys. Chem. B* **2003**, *107*, 12303.

(13) Zahn, D. *Chem. Phys.* **2004**, *300*, 79.

(14) Zahn, D. *Chem. Phys. Lett.* **2004**, *383*, 134.

(15) Zahn, D. *Eur. J. Org. Chem.* **2004**, *19*, 4020.

(16) Pliego, J. R., Jr. *Chem. Phys.* **2004**, *306*, 273.

(17) Cascella, M.; Raugei, S.; Carloni, P. *J. Phys. Chem. B* **2004**, *108*, 369.

(18) Slebocka-Tilk, H.; Sauriol, F.; Monette, M.; Brown, R. S. *Can. J. Chem.* **2002**, *80*, 1343.

(19) Gorb, L.; Asensio, A.; Tunon, I.; Ruiz-Lopez, M. F. *Chem.-Eur. J.* **2005**, *11*, 6743.

(20) Strajbl, M.; Florian, J.; Warshel, A. *J. Am. Chem. Soc.* **2000**, *122*, 5354.

(21) March, J. *Advanced Organic Chemistry.* Wiley: New York, 1985.

(22) Oie, T.; Loew, G. H.; Burt, S. K.; Binkley, J. S.; MacElroy, R. D. *J. Am. Chem. Soc.* **1982**, *104*, 6169.

(23) Jensen, J. H.; Baldridge, K. K.; Gordon, M. S. *J. Phys. Chem.* **1992**, *96*, 8340.

(24) Kallies, B.; Mitzner, R. *J. Mol. Model.* **1998**, *4*, 183.

12652 *J. Phys. Chem. A, Vol. 110, No. 46, 2006*

Xiong and Zhan

(25) Antonczak, S.; Ruiz-Lopez, M. F.; Rivail, J.-L. *J. Mol. Model.* **1997**, *3*, 434.

(26) Smith, C. R.; Yates, K. *Can. J. Chem.* **1972**, *50*, 771.

(27) Kresge, A. J.; Fitzgerald, P. H.; Chiang, Y. *J. Am. Chem. Soc.* **1973**, *96*, 4698.

(28) Hori, K.; Kamimura, A.; Ando, K.; Mizumura, M.; Ihara, Y. *Tetrahedron* **1997**, *53*, 4317.

(29) Voityuk, A. A.; Bliznyuk, A. A. *Bull. Acad. Sci. USSR, Div. Chem. Sci. (Engl. Transl.)* **1989**, *38*, 1635.

(30) Alagona, G.; Scrocco, E.; Tomasi, J. *J. Am. Chem. Soc.* **1975**, *97*, 6976.

(31) Weiner, S. J.; Singh, U. C.; Kollman, P. A. *J. Am. Chem. Soc.* **1985**, *107*, 2219.

(32) Cascella, M.; Raugei, S.; Carloni, P. *J. Phys. Chem. B* **2004**, *108*, 369.

(33) Xiong, Y.; Zhan, C.-G. *J. Central China Normal Univ., Nat. Sci.* **2004**, *38*, 344.

(34) Blumberger, J.; Ensing, B.; Klein, M. L. *Angew. Chem., Int. Ed.* **2006**, *45*, 2893.

(35) Blumberger, J.; Klein, M. L. *Chem. Phys. Lett.* **2006**, *422*, 210.

(36) Zhan, C.-G.; Landry, D. W.; Ornstein, R. L. *J. Am. Chem. Soc.* **2000**, *122*, 2621.

(37) Zhan, C.-G.; Bentley, J.; Chipman, D. M. *J. Chem. Phys.* **1998**, *108*, 177.

(38) Zhan, C.-G.; Chipman, D. M. *J. Chem. Phys.* **1998**, *109*, 10543.

(39) Zhan, C.-G.; Chipman, D. M. *J. Chem. Phys.* **1999**, *110*, 1611.

(40) Zhan, C.-G.; Landry, D. W.; Ornstein, R. L. *J. Phys. Chem. A* **2000**, *104*, 7672.

(41) Zhan, C.-G.; Dixon, D. A. *J. Phys. Chem. A* **2001**, *105*, 11534.

(42) Zhan, C.-G.; Dixon, D. A. *J. Phys. Chem. A* **2002**, *106*, 9737.

(43) Zhan, C.-G.; Dixon, D. A. *J. Phys. Chem. B* **2003**, *107*, 4403.

(44) Zhan, C.-G.; Dixon, D. A. *J. Phys. Chem. A* **2004**, *108*, 2020.

(45) Zhan, C.-G.; Landry, D. W. *J. Phys. Chem. A* **2001**, *105*, 1296.

(46) Zheng, F.; Zhan, C.-G.; Ornstein, R. L. *J. Chem. Soc., Perkin Trans. 2* **2001**, 2355.

(47) Zheng, F.; Zhan, C.-G.; Ornstein, R. L. *J. Phys. Chem. B* **2002**, *106*, 717.

(48) Zhan, C.-G.; Dixon, D. A.; Sabri, M. I.; Kim, M.-S.; Spencer, P. S. *J. Am. Chem. Soc.* **2002**, *124*, 2744.

(49) Dixon, D. A.; Feller, D.; Zhan, C.-G.; Francisco, S. F. *J. Phys. Chem. A* **2002**, *106*, 3191.

(50) (a) Zhan, C.-G.; Norberto de Souza, O.; Rittenhouse, R.; Ornstein, R. L. *J. Am. Chem. Soc.* **1999**, *121*, 7279. (b) Zhan, C.-G.; Zheng, F. *J. Am. Chem. Soc.* **2001**, *123*, 2835. (c) Dixon, D. A.; Feller, D.; Zhan, C.-G.; Francisco, S. F. *Int. J. Mass Spectrom.* **2003**, *227*, 421. (d) Zhan, C.-G.; Dixon, D. A.; Spencer, P. S. *J. Phys. Chem. B* **2003**, *107*, 2853. (e) Zhan, C.-G.; Dixon, D. A.; Spencer, P. S. *J. Phys. Chem. B* **2004**, *108*, 6098. (f) Chen, X.; Zhan, C.-G. *J. Phys. Chem. A* **2004**, *108*, 3789. (g) Chen, X.; Zhan, C.-G. *J. Phys. Chem. A* **2004**, *108*, 6407. (h) Xiong, Y.; Zhan, C.-G. *J. Org. Chem.* **2004**, 69, 8451. (i) Zhan, C.-G.; Deng, S.-X.; Skiba, J. G.; Hayes, B. A.; Tschampel, S. M.; Shields, G. C.; Landry, D. W. *J. Comput. Chem.* **2005**, *26*, 980.

(51) Tomasi, J.; Persico, M. *Chem. Rev.* **1994**, *94*, 2027.

(52) Mejias, J. A.; Lago, S. *J. Chem. Phys.* **2000**, *113*, 7306.

(53) Cramer, C. J.; Truhlar, D. G. In *Solvent Effects and Chemical Reactions*; Tapia, O., Bertran, J., Eds.; Kluwer: Dordrecht, The Netherlands, 1996; p 1.

(54) Chipman, D. M. *J. Chem. Phys.* **2000**, *112*, 5558.

(55) Barone, V.; Cossi, M.; Tomasi, J. *J. Chem. Phys.* **1997**, *107*, 3210.

(56) Tomasi, J.; Mennucci, B.; Cances, E. *J. Mol. Struct. (THEOCHEM)* **1999**, *464*, 211.

(57) Cancès, E.; Mennucci, B. *J. Chem. Phys.* **2001**, *114*, 4744.

(58) Cossi, M.; Rega, N.; Scalmani, G.; Barone, V. *J. Chem. Phys.* **2001**, *114*, 5691.

(59) Chipman, D. M. *J. Chem. Phys.* **2002**, *116*, 10129.

(60) (a) Chen, F.; Chipman, D. M. *J. Chem. Phys.* **2003**, *119*, 10289. (b) Chipman, D. M. *Theor. Chem. Acc.* **2004**, *111*, 61.

(61) Tawa, G. J.; Topol, I. A.; Burt, S. K.; Caldwell, R. A.; Rashin, A. A. *J. Chem. Phys.* **1998**, *109*, 4852.

(62) Topol, I. A.; Tawa, G. J.; Burt, S. K.; Rashin, A. A. *J. Chem. Phys.* **1999**, *111*, 10998.

(63) Becke, A. D. *J. Chem. Phys.* **1993**, *98*, 5648.

(64) Lee, C.; Yang, W.; Parr, R. G. *Phys. Rev. B* **1988**, *37*, 785.

(65) Stephens, P. J.; Devlin, F. J.; Chabalowski, C. F.; Frisch, M. J. *J. Phys. Chem.* **1994**, *98*, 11623.

(66) (a) Gonzalez, C.; Schlegel, H. B. *J. Chem. Phys.* **1989**, *90*, 2154. (b) Gonzalez, C.; Schlegel, H. B. *J. Phys. Chem.* **1990**, *94*, 5523.

(67) Zhan, C.-G.; Landry, D. W.; Ornstein, R. L. *J. Am. Chem. Soc.* **2000**, *122*, 1522.

(68) Frisch, M. J.; Trucks, G. W.; Schlegel, H. B.; Scuseria, G. E.; Robb, M. A.; Cheeseman, J. R.; Montgomery, J. A., Jr.; Vreven, T.; Kudin, K. N.; Burant, J. C.; Millam, J. M.; Iyengar, S. S.; Tomasi, J.; Barone, V.; Mennucci, B.; Cossi, M.; Scalmani, G.; Rega, N.; Petersson, G. A.; Nakatsuji, H.; Hada, M.; Ehara, M.; Toyota, K.; Fukuda, R.; Hasegawa, J.; Ishida, M.; Nakajima, T.; Honda, Y.; Kitao, O.; Nakai, H.; Klene, M.; Li, X.; Knox, J. E.; Hratchian, H. P.; Cross, J. B.; Adamo, C.; Jaramillo, J.; Gomperts, R.; Stratmann, R. E.; Yazyev, O.; Austin, A. J.; Cammi, R.; Pomelli, C.; Ochterski, J. W.; Ayala, P. Y.; Morokuma, K.; Voth, G. A.; Salvador, P.; Dannenberg, J. J.; Zakrzewski, V. G.; Dapprich, S.; Daniels, A. D.; Strain, M. C.; Farkas, O.; Malick, D. K.; Rabuck, A. D.; Raghavachari, K.; Foresman, J. B.; Ortiz, J. V.; Cui, Q.; Baboul, A. G.; Clifford, S.; Cioslowski, J.; Stefanov, B. B.; Liu, G.; Liashenko, A.; Piskorz, P.; Komaromi, I.; Martin, R. L.; Fox, D. J.; Keith, T.; Al-Laham, M. A.; Peng, C. Y.; Nanayakkara, A.; Challacombe, M.; Gill, P. M. W.; Johnson, B.; Chen, W.; Wong, M. W.; Gonzalez, C.; Pople, J. A. *Gaussian 03*, Revision A.1; Gaussian, Inc.: Pittsburgh, PA, 2003.

(69) Aprà, E.; Windus, T. L.; Straatsma, T. P.; Bylaska, E. J.; de Jong, W.; Hirata, S.; Valiev, M.; Hackler, M.; Pollack, L.; Kowalski, K.; Harrison, R.; Dupuis, M.; Smith, D. M. A.; Nieplocha, J.; Tipparaju V.; Krishnan, M.; Auer, A. A.; Brown, E.; Cisneros, G.; Fann, G.; Fruchtl, H.; Garza, J.; Hirao, K.; Kendall, R.; Nichols, J.; Tsemekhman, K.; Wolinski, K.; Anchell, J.; Bernholdt, D.; Borowski, P.; Clark, T.; Clerc, D.; Dachsel, H.; Deegan, M.; Dyall, K.; Elwood, D.; Glendening, E.; Gutowski, M.; Hess, A.; Jaffe, J.; Johnson, B.; Ju, J.; Kobayashi, R.; Kutteh, R.; Lin, Z.; Littlefield, R.; Long, X.; Meng, B.; Nakajima, T.; Niu, S.; Rosing, M.; Sandrone, G.; Stave, M.; Taylor, H.; Thomas, G.; van Lenthe, J.; Wong, A.; Zhang, Z. *NWChem, A Computational Chemistry Package for Parallel Computers*, Version 4.7; Pacific Northwest National Laboratory: Richland, WA, 2005.

(70) Schmidt, M. W.; Baldridge, K. K.; Boatz, J. A.; Elbert, S. T.; Gordon, M. S.; Jensen, J. H.; Koseki, S.; Matsunaga, N.; Nguyen, K. A.; Su, S. J.; Windus, T. L.; Dupuis, M.; Montgomery, J. A. *J. Comput. Chem.* **1993**, *14*, 1347.

(71) Kirsch, J. F. In *Isotope Effects on Enzyme Catalyzed Reactions*; Cleland, W. W., O'Leary, M. H., Northrup, D. B., Eds.; University Park Press: Baltimore, MD, 1977; pp 100−121.

(72) (a) Bolton, P. D. *Aust. J. Chem.* **1966**, *19*, 1013. (b) Bolton, P. D.; Jackson, G. L. *Aust. J. Chem.* **1971**, *24*, 969.